JOURNAL OF SOLID STATE CHEMISTRY 50, 273–280 (1983)

Phase Equilibria of the Mn–Fe–O System (Fe/Mn = 2)

TOSHIHIDE TSUJI, YAMATO ASAKURA, TOSHIYUKI YAMASHITA, AND KEIJI NAITO

Department of Nuclear Engineering, Faculty of Engineering, Nagoya University, Furo-cho, Chikusa-ku, Nagoya 464, Japan

Received October 26, 1982, in final form July 28, 1983

Phase equilibria of the Mn–Fe–O system (Fe/Mn = 2) were studied in the temperature range 1223–1393 K and in oxygen partial pressure from 10^{-1} to 10^5 Pa by measuring the electrical conductivity and the weight of the sample. The standard enthalpy and entropy changes per one mole oxygen for the phase boundary reaction between spinel and spinel + hematite were calculated from thermogravimetric data. A slight break in the plots between the oxygen partial pressure and weight change at constant temperature was observed in the single phase of manganese ferrite, where the lattice constant also showed a break in the plots of lattice constant against oxygen partial pressure. The oxygen potentials were calculated by assuming that the break point in the plots between the oxygen partial pressure and weight change is the stoichiometric composition of manganese ferrite.

1. Introduction

Manganese ferrites as well as manganese zinc ferrites are some of the magnetic materials widely used for electronic applications, and it is known that their magnetic and electrical properties are strongly influenced by the procedures of preparation and fabrication (*1*). However, the thermodynamic properties of manganese ferrites at high temperatures are not well known and the phase boundaries in the Mn–Fe–O system are not fully established.

Muan and Sōmiya (*2*) have extensively studied the phase relations of the iron oxide–manganese oxide system in the temperature range 1073–1858 K in air ($P_{O_2} = 2.1 \times 10^4$ Pa), and found the presence of the following phases: spinel solid solution ($(Fe,Mn)_3O_4$), hematite solid solution (α-Fe_2O_3 with some manganese oxide dissolved in its structure), bixbyite solid solution (α-Mn_2O_3 with some iron oxide dissolved in its structure), tetragonal hausmannite solid solution (Mn_3O_4 with some iron oxide dissolved in its structure). They proposed a phase diagram of the Mn–Fe–O system (in the form of a pseudobinary diagram of the oxides) in the temperature range from 873 to 1873 K in air. Bergstein and Kleinert (*3*) studied the effect of oxygen partial pressures ($P_{O_2} = 2.0 \times 10^4$, 3.3×10^2, and 53 Pa) on the phase boundaries of the two-phase region (sesquioxide + spinel) in the Mn–Fe–O system (Mn/Fe = 0.5, 0.75, 1.0, and 1.285) by means of high temperature X-ray diffraction and dilatometric measurements. Ono *et al.* (*4*) established the isobaric phase diagrams in air and in helium ($P_{O_2} = 1.99$ Pa) in the temperature range 1073–1573 K and the phase diagram of an isothermal section at 1173 K.

0022-4596/83 $3.00

They also determined the equilibrium relationship between spinel and manganowüstite at 1173 K.

As for the nonstoichiometry of oxygen in manganese ferrites, Wickham (5) determined the excess oxygen δ as a function of the ratio of Mn/(Fe+Mn) for $Mn_xFe_{3-x}O_{4+\delta}$ in the temperature range 1250–1673 K in air. He found that the substitution of a small amount of manganese decreases δ considerably, and for a given atomic fraction of manganese δ decreases with increasing equilibrium temperature. Tanaka (6) measured the lattice constants of the quenched $Mn_xFe_{3-x}O_{4+\delta}$ samples (x = 0.950, 0.916, 0.861, or 0.802) equilibrated at 1473, 1573, and 1623 K in the oxygen partial pressure range 1–10^5 Pa by X-ray diffractometry at room temperature. He found a maximum in the relation of lattice constant versus oxygen partial pressure curve at each temperature, and the maximum was suggested to be the lattice constant at nearly stoichiometric composition.

In this paper, the phase relation of the Mn–Fe–O system (Fe/Mn = 2) was studied in the temperature range 1223–1393 K and in oxygen partial pressure from 10^{-1} to 10^5 Pa by measuring the electrical conductivity and weight of sample, and each phase was confirmed by X-ray diffractometry and by electron probe microanalysis. The oxygen potentials in a single phase of $MnFe_2O_{4+\delta}$ spinel at high temperatures were calculated from thermogravimetric data.

2. Experimental

2.1. Sample

Manganese carbonate ($MnCO_3$) and ferric oxide (Fe_2O_3), both with high purity, were mixed in metal composition Fe/Mn = 2 in an agate mortar and the mixture was heated at 973 K for about 10 hr. Then it was cooled to room temperature and mixed again carefully and pressed in a 7-mm circular die at about 20 kg/mm^2 to make a pellet.

For thermogravimetry and X-ray diffractometry, the pellet was sintered at 1523 K in air for about 100 hr and pulverized again and used for the measurements.

For electrical conductivity measurement, the pellet was preannealed at 1073 K in air for about 3 hr and cooled. Then four holes of 0.3-mm diameter were drilled in a line and a platinum wire of 0.3-mm diameter was inserted into each hole as an electrode (7). The pellet was sintered in the same way as the samples for thermogravimetry and X-ray diffractometry.

2.2. Apparatus

A schematic diagram of the apparatus used in this study is shown in Fig. 1. Both argon and oxygen gases were purified by

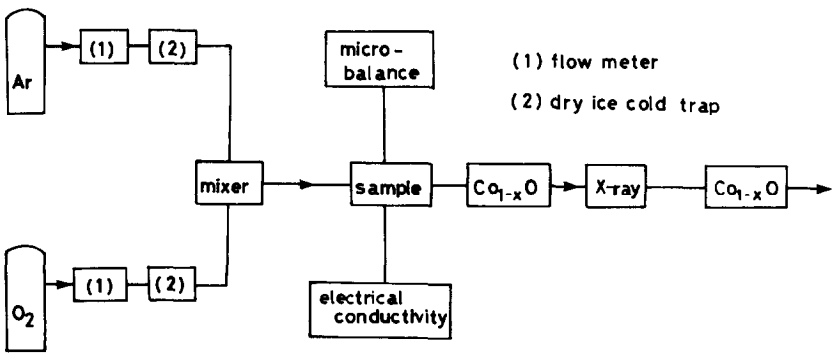

FIG. 1. A schematic diagram of the apparatus.

passing through a dry ice cold trap to remove water vapor. The oxygen partial pressure was controlled by adjusting the mixing ratio of Ar and O_2 gases in the oxygen partial pressure range 10^{-1}–10^5 Pa, and monitored by measuring the electrical resistance of $Co_{1-x}O$ (*8*). The $Co_{1-x}O$ monitors were placed before and after an X-ray diffractometer as shown in Fig. 1.

The samples with the same composition for both electrical conductivity and gravimetric measurements were placed close to each other in the same furnace. The temperature was measured by a Pt–Pt 13% Rh thermocouple placed near the samples, and the temperature of the furnace was regulated within ±2 K by an electronic controller. The electrical conductivity was measured by means of the four inserted wires method as described in the previous paper (*7*). This method is not precise enough to measure absolute values of electrical conductivity, but it is adequate to indicate the relative variations (*7*).

The gravimetric measurement was carried out with a microbalance. The weight of a powdered sample was about 500 mg, and changes in the weight could be read down to ±5 μg, which corresponds approximately to a change of ±0.00005 in O/(Mn + 2Fe) ratio. Measurements of the electrical conductivity and the weight change of samples were made by decreasing oxygen partial pressure, and then increasing it, and both were in good agreement in the single phase of spinel and in the two-phase region of spinel and hematite. When reduction and oxidation reactions are in agreement reversibly, we concluded that the equilibrium was achieved. Equilibrium was usually reached within 4–8 hr. However, a hysteresis was observed near the phase boundary where three phases of bixbyite, hematite, and spinel coexist. Equilibrium could not be achieved within a reasonable period of time.

High temperature X-ray diffraction data were obtained with a diffractometer equipped with a platinum resistance furnace using Fe$K\alpha$ radiation. A very thin layer of a finely pulverized sample was wetted with acetone on a sample holder (Pt 10% Rh alloy), which also served as a heater. Before measurement, the acetone was removed slowly in a vacuum at about 373 K. The temperature was measured with a Pt–Pt 13% Rh thermocouple welded on the back of the sample holder. Reflections of higher angles (511), (440), (533), and (731) were used for the measurement of lattice constants. The imprecision of the measurement of lattice constants was ±0.0003 Å.

The electron probe microanalysis was carried out for both manganese and iron by using quartz as an analyzing crystal.

3. Results and Discussion

3.1. Phase Equilibria of the Mn–Fe–O System

Preliminary measurement of electrical conductivity has been carried out by varying oxygen partial pressure at a constant temperature. Figure 2 shows plots of the electrical conductivity against oxygen partial pressure at 1273 K. The electrical conductivity was constant until 10^4 Pa as oxygen partial pressure decreased, then increased with decreasing oxygen partial pressure as shown by a solid line in the figure and again became nearly constant. When the oxygen partial pressure increased, the electrical conductivity followed the same line below $10^{3.7}$ Pa, but then showed hysteresis as shown by a dotted line in Fig. 2. Three phases of spinel, hematite, and bixbyite were observed by high temperature X-ray diffractometry in the region shown in the dotted line, while only two phases of hematite and bixbyite were detected in the region of the solid line. The hysteresis observed by the electrical con-

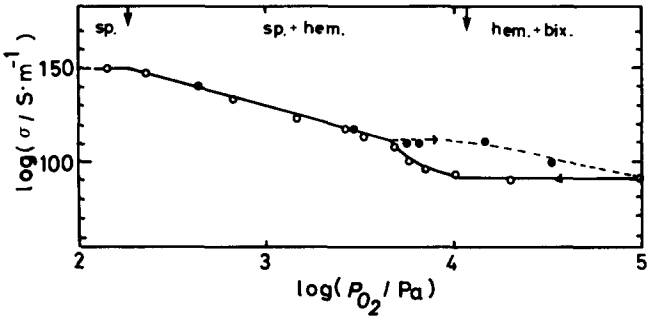

FIG. 2. The log σ vs the oxygen partial pressure at 1273 K. The hysteresis was observed as shown by solid and dotted lines in the figure. The values of electrical conductivity measured in the direction of reduction and oxidation are shown by circles and dots in the figure, respectively.

ductivity measurement shown in Fig. 2 can be explained on the basis of the results of high temperature X-ray diffractometry. As the electrical conductivity of spinel is higher than that of a mixture of hematite and bixbyite, the electrical conductivity in the direction of oxidation is higher than that in the direction of reduction. It is suggested, therefore, that the system does not reach the equilibrium state yet in the region where hysteresis is observed, but it can be claimed that the reduction experiment path is closer to equilibrium than the oxidation one, since the phase rule prohibits the coexistence of three phases at equilibrium in the wide range of oxygen partial pressure at a constant temperature.

Figure 3 shows plots of electrical conductivity and O/(Mn + 2Fe) ratio against oxygen partial pressure at 1273 K. In this figure, the O/(Mn + 2Fe) ratio was calculated from weight change of the sample by assuming a break in the plots between weight and oxygen partial pressure in $MnFe_2O_{4+\delta}$ spinel phase to correspond stoichiometric composition as will be discussed later. It is seen from Fig. 3 that both values of electrical conductivity and O/(Mn + 2Fe) ratio are reversible for the variation of oxygen partial pressure below $10^{3.3}$ Pa. Thermogravimetry as well as electrical conductivity measurement showed hysteresis as shown in dotted line in Fig. 3. When the samples were kept for 1 month in pure oxygen gas at 1273 K, the values of O/(Mn + 2Fe) and electrical conductivity gradually approached the values measured in the direction of reduction. It is also seen in Fig. 3 that the oxygen partial pressure where hysteresis in the direction of oxidation begins

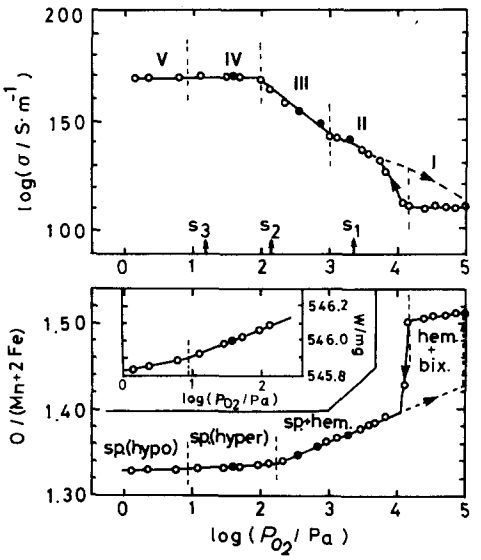

FIG. 3. The log σ and the O/(Mn + 2Fe) ratio vs the oxygen partial pressure at 1273 K. The values of electrical conductivity and O/(Mn + 2Fe) ratio measured in the reduction and oxidation experiments are shown by circles and dots in the figure, respectively.

is higher for the case of thermogravimetry than that for electrical conductivity measurement. This may be explained by the fact that equilibrium could be reached faster in powdered sample used for thermogravimetry than in pellet for electrical conductivity measurement. Five regions may be designated from the dependence of oxygen partial pressure of electrical conductivity and O/(Mn + 2Fe) ratio as shown in Fig. 3. In the region I, the oxygen partial pressure dependences of both electrical conductivity and O/(Mn + 2Fe) ratio were very small, and high temperature X-ray diffraction study showed the presence of both bixbyite and hematite phases. Therefore, the region I should be the two-phase region of bixbyite and hematite. As seen from Fig. 3, the weight of the sample near the boundary between regions I and II changed very sharply, and a spinel instead of a bixbyite was observed from high temperature X-ray diffraction measurement. At the phase boundary, the phases of hematite and bixbyite may be coexisting with the phases of spinel and hematite, where the degree of freedom of the system is zero. The ratio of O/(Mn + 2Fe), thus, should jump in a constant oxygen partial pressure as expected from the phase rule. Although the values of O/(Mn + 2Fe) ratio decreased monotonically at the boundary between regions II and III and high temperature X-ray profiles still showed the presence of two phases of spinel and hematite, an anomaly in the electrical conductivity measurement was observed at the boundary as seen from Fig. 3. The difference between phases II and III may be related to the difference in distribution of hematite and spinel in a sample as will be discussed later. In the regions IV and V, only a spinel phase was observed by high temperature X-ray diffractometry. The dependences of electrical conductivity and O/(Mn + 2Fe) ratio against oxygen partial pressure are very small, but the slope of the plots of weight against oxygen partial pressure varies at boundary between the regions IV and V as seen in Fig. 3. So the regions IV and V may be regarded as hyper- and hypostoichiometric manganese ferrites, respectively.

To confirm the aforementioned assignment, X-ray diffractometry and electron probe microanalysis were carried out. Three powdered samples equilibrated at 1273 K and at different oxygen partial pressures S_1, S_2, and S_3 shown in Fig. 3, were quenched rapidly into ice temperature. A room temperature X-ray diffractometry showed that sample S_1 was a mixture of spinel and hematite, whereas samples S_2 and S_3 were spinel alone. Since the sample S_2 is very near the phase boundary between regions III and IV, it may be difficult to detect the presence of hematite.

The concentration profiles for both Fe and Mn in the samples S_1, S_2, and S_3 obtained by electron probe microanalysis are shown in Fig. 4, where a distance of about 50 μm is scanned. It is observed from Fig. 4 that (1) the concentrations of manganese and iron are nearly constant for all regions scanned in the samples S_2 and S_3, whereas

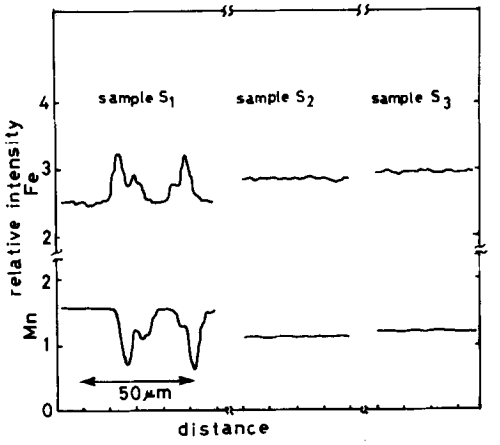

FIG. 4. The concentration profiles obtained by electron probe microanalysis for both Fe and Mn in the samples S_1, S_2, and S_3 which were equilibrated at 1273 K and at different oxygen partial pressures shown in Fig. 3.

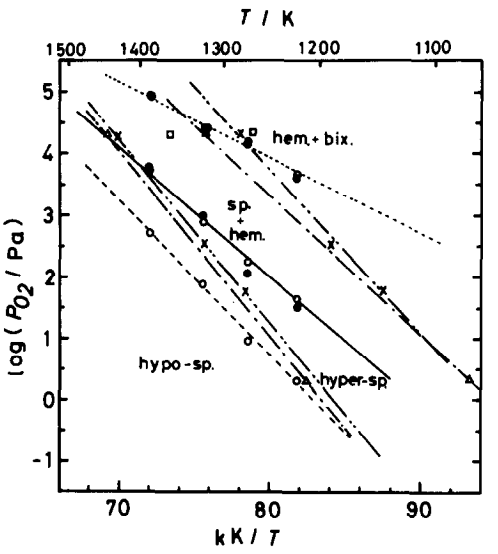

FIG. 5. The oxygen potential diagram which is prepared from the electrical conductivity and thermogravimetric measurements: □, Ref. (*2*); ×, Ref. (*3*); △, Ref. (*4*); ○, thermogravimetry; ●, electrical conductivity measurement.

this is not the case for some regions in the sample S_1, and (2) the intensity of manganese decreases in the place where the intensity of iron increases, as seen clearly in the sample S_1. Case (1) indicates that no deposition of hematite in spinel is detected within a resolution of 1 μm, while case (2) indicates the occurrence of the deposition. It may be concluded from room temperature X-ray diffractometry and electron probe microanalysis that the sample S_1 is a mixture of spinel and hematite, but samples S_2 and S_3 do not show any evidence of a deposition of hematite. If the spinel and hematite in a sample are distributed homogeneously, the electrical conductivity of a mixture of spinel and hematite may vary continuously with the oxygen partial pressure. However, if the spinel in a mixture is formed heterogeneously, the electrical conductivity of the heterogeneous mixture may be higher than that of a homogeneous mixture, since spinel has higher electrical conductivity than hematite in the mixture and the deposition of spinel phase may make a short path for the electric conduction. The anomaly in electrical conductivity at the boundary between regions II and III as shown in Fig. 3 may be due to the heterogeneous distribution of hematite and spinel.

Figure 5 shows the oxygen potential diagram prepared from electrical conductivity measurement and thermogravimetry, where previous results (*2–4*) calculated by the present authors from their pseudo-binary phase diagram (Temperature–Mn/Fe ratio at a constant oxygen partial pressure) are also shown. The solid line represents the phase boundary of two phases (spinel and spinel + hematite) which is obtained from both oxidation and reduction data. The dotted line shows a tentative phase boundary of three phases (spinel + hematite and hematite + bixbyite) which is obtained from reduction data alone. The phase boundary of two phases (spinel and spinel + hematite) obtained by the present authors from thermogravimetry and electrical conductivity measurements are in good agreement as seen from the figure. The results by Bergstein and Kleinert (*3*) and those by Ono *et al.* (*4*) are in fairly good agreement with the present study at high temperatures, but not in agreement at low temperatures. From the facts that their data agree well with our present results at high temperatures and the present results are obtained reversibly for variation of oxygen partial pressure, the data by Bergstein and Kleinert (*3*) and those by Ono *et al.* (*4*) might be out of equilibrium at low temperatures.

Since the linearity at the regions II and III by thermogravimetry is better than that by electrical conductivity measurement as seen in Fig. 3, the oxygen partial pressure for phase boundary of two phases by the former is more reliable than that by the latter. Therefore, only thermogravimetric data were used for the calculation of thermodynamic properties for phase boundary

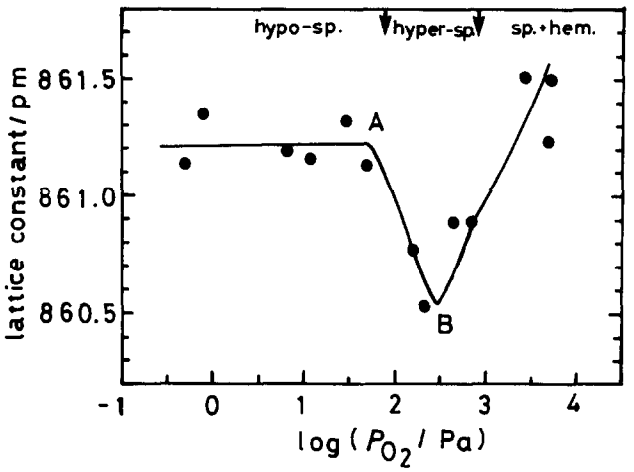

FIG. 6. The lattice constants of manganese ferrite, $MnFe_2O_{4+\delta}$, as a function of oxygen partial pressure at 1323 K.

reaction of two phases. The standard enthalpy change $\Delta H^\circ_{O_2}$ per 1 mole O_2 for the phase boundary reaction of two phases was calculated from the slope of straight line for the phase boundary by thermogravimetry shown in Fig. 5. The standard entropy change $\Delta S^\circ_{O_2}$ per 1 mole O_2 for the phase boundary reaction was evaluated from the slope of the oxygen potential against temperature by thermogravimetry. The standard enthalpy and entropy changes per 1 mole O_2 for the phase boundary reaction

$$\text{Sp.}(MnFe_2O_{4+\delta}) + O_2 \rightleftarrows \text{Sp.}((Fe,Mn)_3O_4) + \text{Hem.}((Fe,Mn)_2O_3)$$

are -414 ± 11 kJ·mole^{-1} and -274 ± 8 J·K^{-1}·mole^{-1}, respectively.

Probable errors of $\Delta H^\circ_{O_2}$ ($11/414 \times 100 \sim 2.7\%$ error) and $\Delta S^\circ_{O_2}$ ($8/274 \times 100 \sim 2.9\%$ error) were calculated from linear regression by methods of least squares, using thermogravimetric data alone. A major source of error may be caused by measurement of oxygen partial pressure, since the temperature was regulated within ± 2 K ($\sim 0.16\%$ error) and O/(Mn + 2Fe) ratio was observed in the change of ± 0.00005 ($\sim 0.004\%$ error).

3.2. Nonstoichiometric Manganese Ferrite

The lattice constants of $MnFe_2O_{4+\delta}$ as a function of oxygen partial pressure at 1323 K are shown in Fig. 6, where the oxygen partial pressure at phase boundary between spinel and spinel + hematite and that at the stoichiometric composition obtained from Fig. 5 are also given by arrows. The similar behavior for the plots of lattice constant against oxygen partial pressure in a single phase of manganese ferrite has been observed by Tanaka (*6*). He observed from the measurement of oxygen content of sample by an electron probe microanalysis at room temperature that the lattice constant of a sample with a nearly stoichiometric oxygen content, i.e., $\delta = 0$, took a maximum value. It is seen from Fig. 6 that the oxygen partial pressure at the break in the plots between oxygen partial pressure and the O/(Mn + 2Fe) ratio in spinel phase shown in Fig. 3 corresponds to that at point A in Fig. 6. But the minimum in the lattice constant (point B in Fig. 6) does not occur at the alleged boundary curve (see arrow in Fig. 6). The minimum can be caused by the different dependence of lattice constant on oxygen partial pressure in hyper-manganese

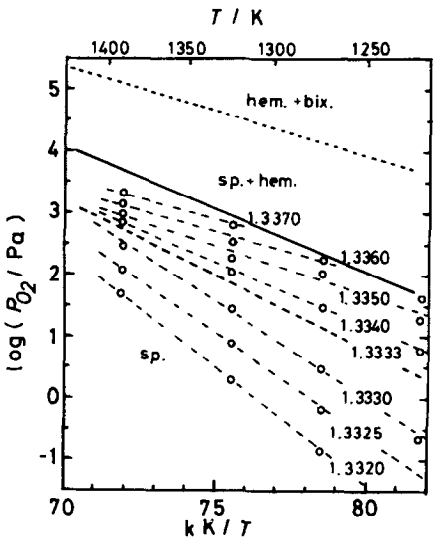

FIG. 7. The log P_{O_2} vs $1/T$ for constant compositions in a single phase of manganese ferrite. The phase boundaries are given by solid and dotted lines, while the broken lines represent the lines of constant compositions within a single phase.

ferrite and in two phase region of hyper-manganese ferrite and hematite. The negative dependence of oxygen partial pressure on lattice constant in hyper-manganese ferrite may be caused by the formation of cation vacancy, which was proposed in the case of Fe_3O_4 (*11*). The fact that a lattice constant of spinel coexisting with hematite increased with increasing oxygen partial pressure can be explained by the substitution of manganese for iron in spinel, accompanying with deposition of hematite, because it has been reported by Muan and Sōmiya (*2*) that d spacing for (440) reflections of the spinel solid solution, $(Mn, Fe)_3O_4$, increased with increasing manganese contents.

Figure 7 shows the logarithm of oxygen partial pressures plotted against reciprocal temperature for constant compositions of manganese ferrite, obtained from isothermal plots of O/(Mn + 2Fe) ratio vs oxygen partial pressure at 1223, 1273, 1323, and 1389 K as shown typically for 1273 K in Fig. 3. The phase boundaries are also given by solid and dotted lines in the figure, while the values at a constant composition within a single phase of manganese ferrite are shown by broken lines. It is observed from Fig. 7 that the slopes of the plots of oxygen partial pressure against $1/T$ are less negative with increasing the O/(Mn + 2Fe) ratio. The similar dependence of O/M (M: metal) ratio is also seen for $Co_{0.165}Fe_{2.835}O_4$ by Macklen (*9*) and for MnZn ferrite by Blank (*10*).

It is seen from Figs. 3 and 6 that the oxygen partial pressure dependence of O/(Mn + 2Fe) ratio and that of lattice constant in the region of hyper-manganese ferrite are larger than those in the region of hypo-manganese ferrite. This may indicate the presence of different defect structures in hyper- and hypo-manganese ferrites.

Acknowledgment

The authors thank Professor H. Sakao, Department of Metallurgical Engineering, Nagoya University, for use of the electron probe microanalysis.

References

1. M. PAULUS, "Preparative Methods in Solid State Chemistry" (P. Hagenmuller, ed.), p. 487. Academic Press, New York (1972).
2. A. MUAN AND S. SŌMIYA, *Amer. J. Sci.* **260,** 230 (1962).
3. A. BERGSTEIN AND P. KLEINERT, *Collect. Czech. Chem. Commun.* **29,** 2549 (1964).
4. K. ONO, T. UEDA, T. OZAKI, Y. UEDA, A. YAMAGUCHI, AND J. MORIYAMA, *J. Japan. Inst. Met. Sendai* **35,** 757 (1971).
5. D. G. WICKHAM, *J. Inorg. Nucl. Chem.* **31,** 313 (1969).
6. T. TANAKA, *Japan. J. Appl. Phys.* **13,** 1235 (1974).
7. T. ISHII, K. NAITO, AND K. OSHIMA, *J. Nucl. Mater.* **35,** 335 (1970).
8. K. NAITO, unpublished.
9. E. D. MACKLEN, *Czech. J. Phys.* **B17,** 376 (1967).
10. J. M. BLANK, *J. Appl. Phys.* **S32,** 378S (1961).
11. P. KOFSTAD, "Nonstoichiometry, Diffusion and Electrical Conductivity in Binary Metal Oxides," Wiley–Interscience, New York (1972).